Conformation, Distance, and Connectivity Effects on Intramolecular Electron Transfer between Phenylene-Bridged Aromatic Redox Centers†

S. V. Rosokha, D.-L. Sun, and J. K. Kochi*

Department of Chemistry, University of Houston, Houston, Texas 77204-5003

Received: July 10, 2001; In Final Form: November 5, 2001

Intramolecular electron transfer in the organic mixed-valence cation radical $\mathbf{D}(\mathrm{ph})_n\mathbf{D}^{+\bullet}$ [where **D** = 2,5-dimethoxy-4-methylphenyl and $(\mathrm{ph})_n$ = poly-p-phenylene] is systematically probed by the structural modification of the molecular *conformation*, separation *distance*, and electronic *connectivity* of the $(\mathrm{ph})_n$ bridge. Cyclic voltammetry and dynamic ESR line broadening studies afford experimental measures of the energy gap (ΔE_{ox}) and the electron-transfer kinetics (k_{ET}) for the $\mathbf{D}/\mathbf{D}^{+\bullet}$ interaction in a series of methyl-substituted, (poly)phenylene, and bridged-modified ph-X-ph (where X = C≡C, CH═CH, O, and CH_2CH_2 inserts or the $(CH_3)_2C$ tiedown) bridges that comprise the groups A−C donors in Chart 1. Theoretical electron-transfer rates are obtained by the application of the Creutz, Newton, and Sutin (CNS) superexchange model (for the calculation of the electron coupling matrix element $\mathbf{H}_{CNS}$) to the diagnostic NIR absorptions that arise from the intramolecular bridge-to-redox center (i.e., br → $\mathbf{D}^{+\bullet}$) charge-transfer transitions. Comparison of the experimental and theoretical electron-transfer rates (k_{ET}) indicate that the CNS model is sufficient to provide a mechanistic basis for including conformation, distance and connectivity effects in the design of (poly)-phenylene bridges for new organic mixed-valence systems.

Introduction

Intramolecular electron exchange in the wholly organic (mixed-valence) system **D**-br-$\mathbf{D}^{+\bullet}$ (where **D** = 2,5-dimethoxy-4-methylphenyl) was by and large successfully treated by the Mulliken−Hush (MH) theory of intervalent (electronic) transition,[1] as originally developed for coupled inorganic redox centers.[2,3] Since the nature of the bridge (br = aliphatic or aromatic) constituted a dominant factor in determining the magnitude of the electronic coupling matrix element **H** between the **D** and $\mathbf{D}^{+\bullet}$ redox centers,[1] we now focus on how the molecular *conformation* and electronic *connectivity* of an aromatic bridge [br = (poly)phenylene] can effectively modulate the intermolecular electron transfer.[4] Critical to this study is the application of the Creutz, Newton, and Sutin (CNS) superexchange formulation to these Robin−Day class II systems, since it will specifically address the electronic coupling of the aromatic (phenylene) bridge directly to the **D** and $\mathbf{D}^{+\bullet}$ redox centers.[5] Accordingly, all the mixed-valence systems selected in Chart 1 for this study constitute structural variants of the basic (**D**/ph) building unit.

The bridge *conformation* is probed in group A donors since the dihedral angle φ around the **D**-br bond increases with methyl substituents− the planar redox center **D** being almost orthogonal to the phenylene bridge in the tetramethyl analogue. Increasing *separation* of the $\mathbf{D}/\mathbf{D}^{+\bullet}$ redox centers is achieved by the series of (poly)phenylene bridges in group B donors. Finally, group C donors maintain the **D**-ph bridge intact, but modify the biphenylene *connectivity* by (a) insertion of acetylenic, ethylenic, and dimethylene spacers and (b) the enforced coplanarization of $(\mathrm{ph})_2$ by the gem-dimethylcarbinyl or $(CH_3)_2C$ (bifunctional) "clamp".

† Part of the special issue "Noboru Mataga Festschrift". Dedicated to Professor Noboru Mataga for his pioneering contributions to our understanding of (fast) electron-transfer processes.

Results

Following the earlier study,[1] the dynamics of intramolecular electron transfer (ET) were serially probed by the combination of cyclic voltammetry, dynamic ESR line broadening, and NIR intervalence absorption of groups A−C donors and their cation radicals.[6]

I. Resonance Interaction of the Redox Centers by Cyclic Voltammetry. The *conformational* effect of the phenylene bridge increased progressively with monomethyl, dimethyl, and tetramethyl substitution in the group A donors. As a result, the (cyclic voltammetric) resonance interaction in $\mathbf{D}(\mathrm{ph})\mathbf{D}^{+\bullet}$ decreased from $\Delta E_{ox} = 2.5$[7] only to 2.1 kcal/mol in the TOL analogue (Table 1), but it then dropped precipitously to $\Delta E_{ox} \approx 0.5$[8] and 0 kcal/mol for the XYL and DUR donors, respectively, in Table 1. Moreover, the planarization of the biphenylene bridge of $\mathbf{D}(\mathrm{ph})_2\mathbf{D}^{+\bullet}$ with $\Delta E_{ox} = 0$ dramatically increased the resonance interaction to $\Delta E_{ox} = 1.4$ kcal/mol in the coplanar FL analogue (Chart 1).

The *distance* dependence [imposed by varying the length of the (poly)phenylene bridge] and the *connectivity* effect (with the additional X-spacer) on the electronic coupling between redox centers were not effectively probed by cyclic voltammetry (CV) since the voltammograms of groups B and C donors uniformly consisted of a single 2e wave that was unresolvable, and the resonance interaction is correspondingly given as $\Delta E_{ox} = 0$ in Table 1, last column.

II. Electronic Interchange by Dynamic ESR Line Broadening. Intramolecular electron-exchange kinetics between **D** and $\mathbf{D}^{+\bullet}$ redox centers in mixed-valence cations **D**-br-$\mathbf{D}^{+\bullet}$ were provided by dynamic ESR simulation[9] of the temperature-dependent line broadening of the ESR spectra, as typically illustrated in Figures 1−3. In some cases, the computer simulation could not be carried out quantitatively owing to unresolved (multiple, small) hyperfine splittings from a (rela-

10.1021/jp012634d CCC: $22.00
Published on Web 02/08/2002

CHART 1: Mixed-Valence Systems (MVS)

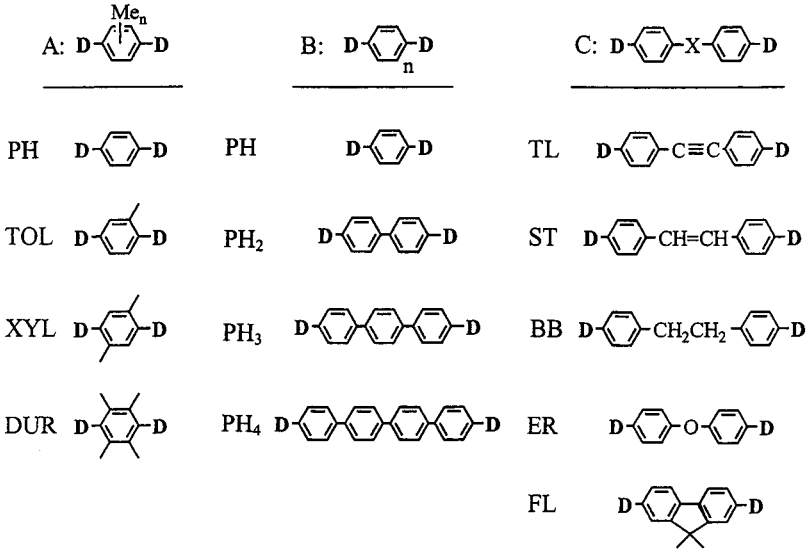

TABLE 1: Cyclic Voltammetry of Group A−C Donors[a]

MVS[b]	E_{br},[c] V vs SCE	$E_{1,2}$,[d] V vs SCE	ΔE_{ox},[e] kcal M^{-1}
PH	2.7[f]	1.15 (1e) 1.26 (1e)	2.5
TOL	2.42[f]	1.16 (1e) 1.25 (1e)	2.1
XYL	2.11[f]	1.17−1.24 (2e)	≈0.5
DUR	1.83[f]	1.21 (2.e)	0
PH_2	1.82	1.18 (2e)	0
PH_3	1.67	1.18 (2e)	0
PH_4	1.66	1.18 (2e)	
FL	1.67	1.13 (1e) 1.19 (1e)	1.4
TL	1.86	1.18 (2e)	0
ST	1.56	1.18 (2e)	0
BB	1.90	1.17 (2e)	0
ER	1.80	1.17 (2e)	0

[a] In dichloromethane containing 0.1 M tetrabuthylammonium hexafluorophosphate as supporting electrolyte, at 20 °C. [b] Mixed-valence systems classified in Chart 1. [c] Reversible oxidation potential of the bridge (as H-br-H). [d] Chemically reversible CV waves 1 and 2; electron change in the CV wave (in parentheses). [e] Entry zero indicates an unresolved 2e CV wave. [f] Reference 18.

tively) large number of nuclei. However for the most part, the semiquantitative simulations were sufficient to provide estimates of the first-order rate constants (k_{ET}) of the electron exchange process, as presented in Table 2.

The *conformational* dependence of the intramolecular electron exchange was shown by the decreasing temperature dependence of the ESR line broadening in Figure 1. At low temperatures (−80 to −100 °C), the ESR spectrum of the monomethyl analogue **D**(tol)$\mathbf{D}^{+\bullet}$ was successfully simulated by using the hyperfine splittings of the mononuclear (model) cation radical **D**(ph)$H^{+\bullet}$, and the first-order rate constant of $k_{ET} = 5 \times 10^6$ s^{-1} was evaluated from the line broadening.[9] The severely broadened ESR spectrum of **D**(tol)$\mathbf{D}^{+\bullet}$ at 20 °C in Figure 1 corresponded to an ET rate constant in the range of 10^8-10^9 s^{-1}. Similarly, the dimethyl and tetramethyl analogues were well-simulated (charge localized on one terminal **D**) with an ET rate constant of less than 3×10^6 s^{-1} at low temperature. Computer simulation of the partially resolved spectra of **D**(xyl)-$\mathbf{D}^{+\bullet}$ and **D**(dur)$\mathbf{D}^{+\bullet}$ at 20 °C in Figure 1 required the introduction of additional (unresolved) hyperfine splitting constants, and k_{ET} could only be estimated to lie in the range of 10^8 s^{-1} (see Experimental Section).

Typical temperature-dependent ESR behavior of the (poly)-phenylene homologues **D**$(ph)_n\mathbf{D}^{+\bullet}$ with $n = 2$, 3, and 4 are

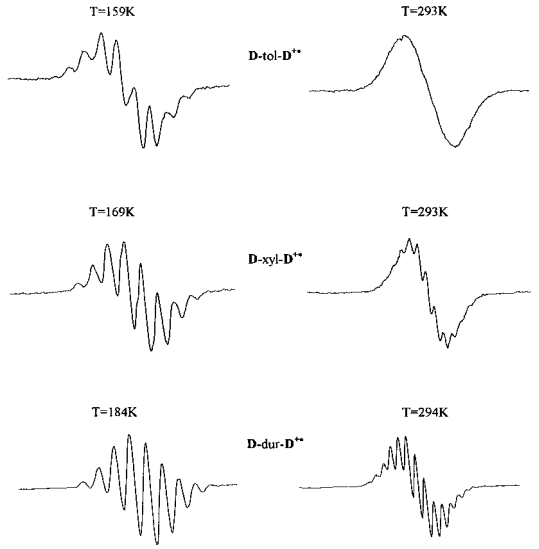

Figure 1. Temperature-dependent ESR line broadening at high (20 °C) and low (−90 to −110 °C) temperatures of tolyl-bridged ($TOL^{+\bullet}$), the xylyl-bridged ($XYL^{+\bullet}$), and the duryl-bridged ($DUR^{+\bullet}$) cation radicals in dichloromethane solution.

shown in Figures 2, left side. At low temperature (−80 to −100 °C), the mostly resolved spectra were simulated with first-order rate constants which decreased from 2×10^7 ($n = 2$) to less than 3×10^6 s^{-1} ($n = 4$). At room temperature, the broadened (unresolved) spectrum of the mono-phenylene analogue gave a rate constant k_{ET} which was estimated to be faster than 10^9 s^{-1} with the help of dynamic ESR simulation.[9] Successive lengthening of the (poly)phenylene bridge led to decreasing rate constants of $k_{ET} = 3 \times 10^9$ s^{-1} ($n = 2$); $10^8 - 10^9$ s^{-1} ($n = 3$) and 3×10^7 s^{-1} ($n = 4$).

Satisfactory simulation of the low-temperature (−100 °C) ESR spectrum of the fluorenyl system **D**(flu)$\mathbf{D}^{+\bullet}$ in Figure 3 required the introduction of additional methyl hyperfine splittings (consistent with the X-ray results that indicated significant charge distribution onto the bridge[10]). The (estimated) rate constant increase at 20 °C (Table 2) derived from a severely broadened ESR spectrum consisting of a single unresolved line. The temperature-dependent ESR spectrum of the tolane and bibenzyl analogues TL and BB, respectively, were not strongly differentiated since unresolved hyperfine splittings were (barely)

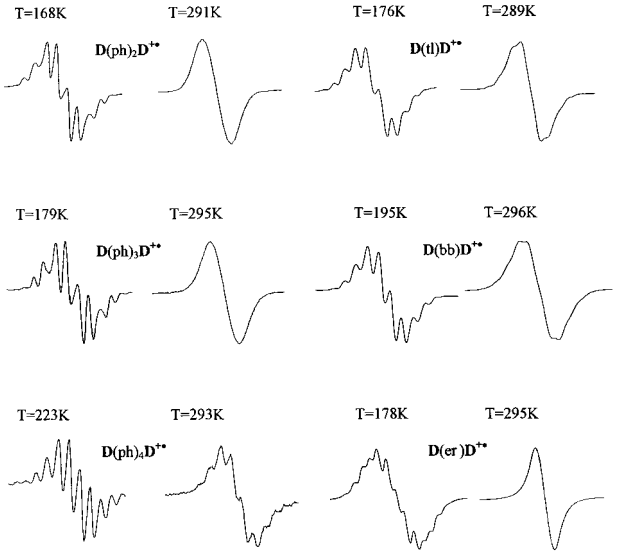

Figure 2. Dynamic ESR line broadening of the (poly)phenylene-bridged cation radicals: left side (top-to-bottom) ($PH_2^{+\bullet}$), ($PH_3^{+\bullet}$), and ($PH_4^{+\bullet}$) at low (−50 to −105 °C) and high (20 °C) temperatures. The effect of the X-insert is similarly shown on the right side for the temperature-dependent line broadening of ($TL^{+\bullet}$), ($BB^{+\bullet}$) and ($ER^{+\bullet}$).

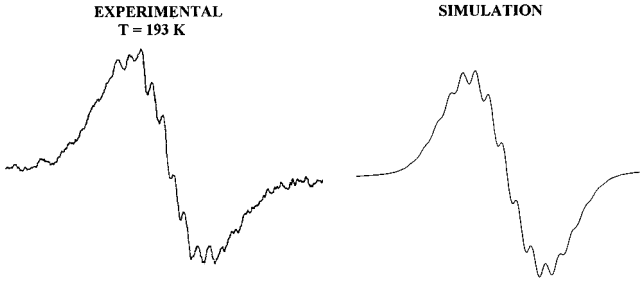

Figure 3. Computer simulation of the experimental ESR line broadening of the fluorenyl-bridged cation radical ($FL^{+\bullet}$) at low (−80°) temperature (see Experimental Section for details).

TABLE 2: Electron-Transfer Rate Constants from Temperature-Dependent ESR Line Broadening[a]

	k_{ET}, s^{-1}			k_{ET}, s^{-1}	
MVS[b]	(−100 °C)	(20 °C)	MVS[b]	(−100 °C)	(20 °C)
PH	10^{10c}	10^{10c}	ST	$10^{8,9}$	$10^{8,9}$
TOL	5×10^6	$10^{8,9}$	FL	5×10^7	$10^{8,9}$
XYL	$<3 \times 10^6$	10^8	ER	$<3 \times 10^6$	$10^{8,9}$
DUR	$<3 \times 10^6$	10^8	TL	5×10^6	10^8
PH_2	2×10^7	3×10^9	BB	$<3 \times 10^6$	5×10^7
PH_3	5×10^6	$10^{8,9}$			
PH_4	$<3 \times 10^6$	3×10^7			

[a] In dichloromethane solution. [b] Mixed-valence system classified in Chart 1. [c] For these fast exchange, see discussion in ref 1.

visible (Figures 2, right side) at high temperature. At the other extreme, the ESR spectrum of the stilbene analogue, **D**(st)$\mathbf{D}^{+\bullet}$ was broadened into a single (unresolved) line at all temperatures between −80 to 20 °C.

III. Intervalence Absorption in the Electronic Spectra. The *conformational* effects on the electronic spectra of the group A mixed-valence cation was shown by the blue shift of the lowest-energy NIR envelope from $\lambda_{max} \sim 1570$ nm in **D**(ph)$\mathbf{D}^{+\bullet}$ to 1180 nm in the TOL analogue (Table 3).[11] Successful deconvolution of these NIR absorption bands (including every mixed-valence cation in group A)[12] by digital subtraction of the components of the corresponding dications[13] revealed the clearly resolved (Gaussian) intervalence bands (see insets in Figure 4), and the NIR values of λ_{IV} are listed in Table 3 (column 7).

TABLE 3: Electronic Spectra of the Cation Radical (CR) and the Dication (DC) of the (poly)Methyl-Substituted Group A System, Together with That of MC = Model Cation Radical (D-br-$H^{+\bullet}$)[a]

MVS[b]		λ_1	ϵ_1	λ_2	ϵ_2	λ_{IV}	ϵ_{IV}
PH	CR	620	2.2	1570	3.9	1570	3.9
	MC	540	7.4	910	2.0		
	DC	550	2.6	910	1.6		
TOL	CR	580	3.5	1180	3.0	1270	0.78
	DC	570	2.8	950	1.5		
XYL	CR	600	2.0	1180	1.6	1250	0.49
	DC	570	1.7	940	0.9		
DUR	CR	680	0.5	1070	0.3	1210	0.22
	DC	650	0.5	940	0.2		

[a] Measured in dichloromethane solution, at 20 °C. Includes only the low-energy absorptions for bands λ_1 and λ_2 in the vis−NIR spectral region. Wavelength (in nm) and extinction coefficient ϵ (in 10^3 M^{-1} cm^{-1}) measured at the absorption maxima. [b] See Chart 1.

Most prominent was the progressive (almost monotonic) attenuation of their oscillator strength (ϵ_{IV}) with increasing methyl substitution of the bridge (see Table 3, column 8). The spectral consequences of *lengthening* the (poly)phenylene bridge in group B cation radicals is shown in Figure 5—especially by the pronounced changes in the NIR envelope. For comparison, the electronic spectra of these mixed-valence cations **D**$(ph)_n\mathbf{D}^{+\bullet}$ were superimposed onto the corresponding spectra of the dications **D**$(ph)_n\mathbf{D}^{2+}$, as well as the cation radicals of the mononuclear models **D**$(ph)_nH^{+\bullet}$. Spectral subtraction (as described above) afforded the resolved (Gaussian) intervalence bands for the (poly)phenylene analogues with $n = 1$ and 2 (Table 4).[14] Since the previous X-ray and ESR analysis of the dication **D**$(ph)_n\mathbf{D}^{2+}$ and mononuclear models **D**$(ph)_nH^{+\bullet}$ established the cationic charge to reside primarily on the $\mathbf{D}^{+\bullet}$ redox centers,[10] the pair of resolved (Vis) bands in Figure 5 were readily assigned to the intramolecular (electronic) transition from the bridge to redox center, i.e., ph $\rightarrow \mathbf{D}^{+\bullet}$ that originated from the filled (phenylene) HOMO and HOMO-1.[15] Such a spectral assignment was also strongly supported in Figure 6 by the marked dependence of the charge-transfer absorption band (ν_{bDCT}) with the ionization potential of the bridge evaluated as the simple (dihydro) parent, i.e., H-br-H.[16] [Indeed, the observed red-shift of these bands with increasing methyl substitution together with their constant energy separation that corresponds to the first and second ionization potential of the bridge moiety[18] also added support to such a charge-transfer spectral assignment.] It is especially noteworthy that the spectral distinction between the intervalence and the charge-transfer absorption essentially disappeared in the (poly)phenylene systems with $n = 3$ and 4, and the electronic spectra of these mixed-valence cation radicals **D**$(ph)_n\mathbf{D}^{+\bullet}$ bore strong resemblance to those of the dications[13] **D**$(ph)_n\mathbf{D}^{2+}$ and the model cation radicals **D**$(ph)_nH^{+\bullet}$.[19]

The biphenylene *connectivity* in group C donors led to distinct intervalence bands (Table 4) when the bridge contained acetylenic (−C≡C−) and ethylenic (−CH═CH−) units, but no or little change was noted in the saturated alkylidene ($-CH_2CH_2-$) or the ethereal (−O−) analogues.

The importance of *planarization* of the biphenylene bridge (by insertion of the difunctional $-(CH_3)_2C-$ tie) had a dramatic effect on the intervalence band, which underwent a strong red shift from $\lambda_{IV} = 1330$ nm in **D**$(ph)_2\mathbf{D}^{+\bullet}$ to 1780 nm in the FL (Chart 1) analogue. [Otherwise, note that the absorption bands of the FL dication showed only a small red shift relative to that of the parent biphenylene analogue **D**$(ph)_2\mathbf{D}^{2+}$, owing to the slightly better donor property of the fluorenyl bridge itself.[20]]

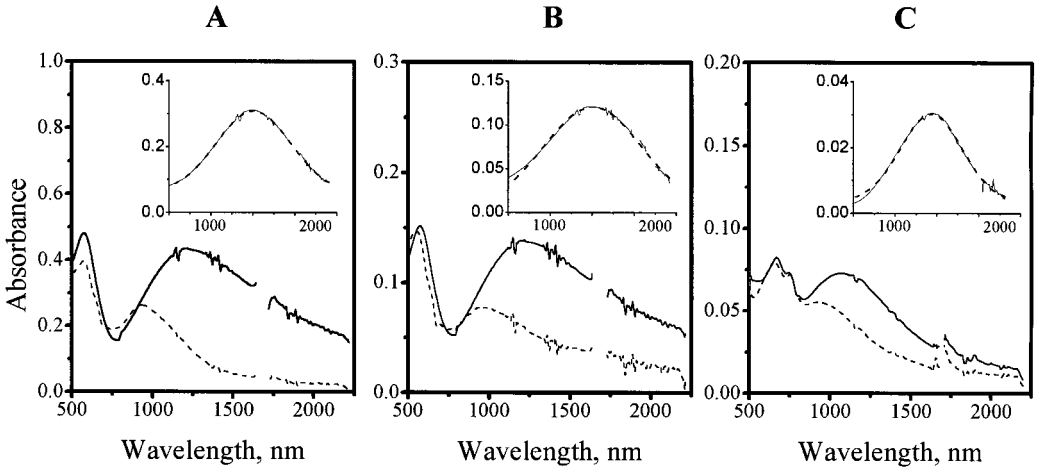

Figure 4. Comparative electronic spectra of the phenylene-bridged cation radical **D**(ph)**D**$^{+\bullet}$ upon substitution with (A) one, (B) two, and (C) four methyl groups (—) relative to the dication (- -). The Gaussian (NIR) intervalence bands obtained by digital subtraction are shown in the inset.

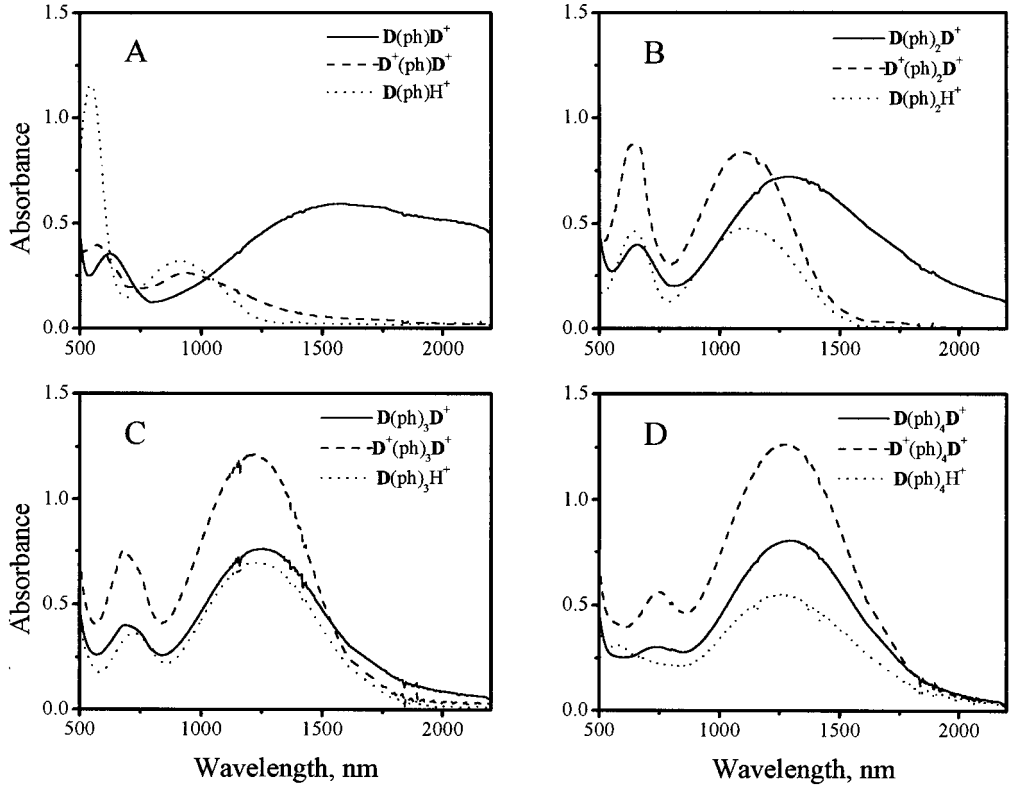

Figure 5. Electronic spectra of the (poly)phenylene-bridged cation radicals CR = **D**(ph)$_n$**D**$^{+\bullet}$ with (A) $n = 1$, (B) $n = 2$, (C) $n = 3$ and (D) $n = 4$ (shown as solid lines) in comparison with corresponding dication DC = **D**(ph)$_n$**D**$^{2+}$ (shown as dashed lines) and the mononuclear cation radical MC = **D**(ph)$_n$H$^{+\bullet}$ (shown as dotted lines).

Discussion

Intramolecular electron transfer in the mixed-valence cation radicals **D**-br-**D**$^{+\bullet}$ is more effective in the aromatic phenylene (-ph-) rather than an aliphatic trimethylene ($-CH_2CH_2CH_2-$) bridge, despite the greater separation between the **D**/**D**$^{+\bullet}$ redox centers.[1] Indeed, the electronic coupling in the phenylene-bridged cation **D**(ph)**D**$^{+\bullet}$ even begins to rival the efficiency achieved in the directly coupled biaryl cation **D**-**D**$^{+\bullet}$.[1] Accordingly, let us first consider how the structural features of (poly)-phenylene bridges in groups A−C donors (Chart 1) can affect the magnitudes of the critical electronic coupling matrix element **H** by the application of the Mulliken−Hush formalism based on the semiclassical two-state model.[2,5]

I. Mulliken−Hush Calculation of the Electronic Coupling Elements in Groups A−C Cation Radicals. For Robin−Day class II (mixed-valence) systems, such as the cation radicals of the donors in Chart 1, the electronic coupling element is evaluated by the Mulliken−Hush expression:

$$\mathbf{H} = 0.0206(\nu_{max}\Delta\nu_{1/2}\epsilon)^{1/2}/r \qquad (1)$$

where the spectral characteristics of the intervalence bands are those listed in Tables 3 and 4.[22] The calculated values of $\mathbf{H}_{MH}$ in Table 5 also obtain with the aid of the separation parameter r from the molecular mechanics calculations based on the Alchemy algorithm (see Experimental Section).

The conformational effect of (poly)methyl substitution on the phenylene bridge is shown in Table 5 by the decreasing values of $\mathbf{H}_{MH}$, which progressive decrease in value from the unsubstituted PH to the tetramethyl (DUR) system. Likewise, the

TABLE 4: Electronic Spectra of Groups B and C Systems and Their Mononuclear Models[a]

MVS		λ_1	ϵ_1	λ_2	ϵ_2	λ_{IV}	ϵ_{IV}
PH_2	CR	660	2.3	1330	4.5	1470	4.2
	MC	640	2.7	1140	3.0		
	DC	640	6.1	1130	5.5		
PH_3	CR	720	2.0	1320	2.3	1490	1.9
	MC	730	2.0	1280	3.9		
	DC	720	4.9	1270	7.5		
PH_4	CR	750	2.0	1290	5.7	*b*	
	MC	750	–	1270	3.8		
	DC	750	3.1	1280	8.7		
TL	CR	710	4.0	1250	4.3	1420	2.6
	DC	720	4.0	1190	7.4		
ST	CR	790	4.6	1830	18.9	1890	17.2
	DC	760	9.6	1540	18.2		
FL	CR	760	3.2	1780	11.4	1780	10.7
	DC	700	4.2	1320	6.6		
BB	CR	540	3.9	1000	1.9	*b*	
	DC	540	7.8	1000	3.8		
ER	CR	615	3.8	1260	4.5	1330	2.3
	DC	615	3.1	1060	3.2		

[a] See Table 3 for notations used. [b] Intervalence band obscured by the bridge-to-$\mathbf{D}^{+\bullet}$ charge-transfer transition.

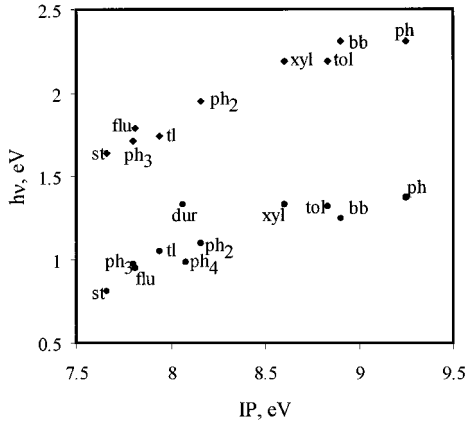

Figure 6. Mulliken correlation of the transition energy of the charge-transfer band (ν_{bDCT}) in the bridged dication **D**-br-$\mathbf{D}^{2+}$ with the ionization potential of the bridge (taken as H-br-H). Lower and upper plots correspond to the HOMO and HOMO-1 transitions, respectively.

TABLE 5: Mulliken–Hush (MH) Calculation of the Electronic Coupling Element

MVS	r,[a] Å	ν_{IV},[b] 10^3 cm^{-1}	$\Delta\nu_{1/2}$,[c] 10^3 cm^{-1}	ϵ_{IV},[b] 10^3 M^{-1} cm^{-1}	$\mathbf{H}_{MH}$,[d] cm^{-1}
PH	8.6	6.37	4.1	3.9	760
TOL	8.6	7.90	4.0	0.78	377
XYL	8.6	7.98	4.7	0.49	325
DUR	8.6	8.28	3.0	0.22	170
PH_2	12.9	6.79	2.5	4.2	430
PH_3	17.2	6.70	2.5	1.9	217
PH_4	21.5				
ER	14.2	7.5	2.0	2.3	270
FL	12.9	5.64	2.6	10.7	630[e]
TL	15.4	7.03	3.3	2.6	327
BB	15.4				
ST	15.4	5.30	2.4	17.2	618[e]

[a] Center-to-center distance for $\mathbf{D}/\mathbf{D}^{+\bullet}$ interaction evaluated by molecular mechanics calculation (see Experimental). [b] From Tables 3 and 4. [c] Bandwidth at half-height. [d] From eq 1. [e] See text.

values of $\mathbf{H}_{MH}$ steadily decrease with the lengthening of the (poly)phenylene bridge $(ph)_n$, such that the intervalence absorption band is no longer visible in the quaterphenylene cation radical with $n = 4$. The latter together with the rather limited temperature-dependent ESR line-broadening in Figure 2 points to $\mathbf{D}(ph)_4\mathbf{D}^{+\bullet}$ as a mixed-valence system near the border between Robin–Day class II/I systems.

The *connectivity* effects in group C cation radicals cover a particularly wide span—$\mathbf{H}_{MH}$ being (i) very small $\mathbf{H}_{MH} \sim 0$ with alkylidene (CH_2CH_2) connector, (ii) moderate $\mathbf{H}_{MH} = 300$ cm^{-1} with the acetylenic (C≡C) and ethereal (O) linkages, and (iii) large $\mathbf{H}_{MH} > 600$ cm^{-1} with the ethylenic group (CH═CH) interposed or the $(CH_3)_2C$ tiedown of the biphenyl rotation. The large calculated $\mathbf{H}_{MH}$ values for the latter were based on their classification as Robin–Day class II cation radicals. However, the X-ray structural analysis of the FL cation radicals[23] shows that considerable positive charge resides on the fluorenyl (flu) bridge, which is supported by the ESR results in Figure 3. Such a conclusion indicates that the energy difference between the cationic charge residing on the terminal **D** groups relative to the charge on the flu bridge is minor,[24] which is indeed consistent with the fact that the oxidation potential of the parent hydrocarbon bridge (fluorene with $E^0_1 = 1.67$ V) is only slightly more than the oxidation potential of the model redox center (2,5-dimethoxytoluene with $E^0_1 = 1.29$ V)[25]. Since the Mulliken–Hush formalism is based on the two state model, eq 1 may no longer being valid, and the calculated values of $\mathbf{H}_{MH}$ for the cation radical of FL (Chart 1) should be considered with this limitation in mind. The same caveat applies to the ethylenic cation radicals (ST), which is also unlikely to be a two-state system owing to the sizable charge distribution on the stilbenoid (st) bridge.[25]

II. Creutz, Newton, and Sutin (CNS) Superexchange Model for the Calculation of the Electronic Coupling Elements. By way of the superexchange formalism, Creutz, Newton, and Sutin[5] showed recently that the metal–metal coupling element **H** in weakly interacting ligand-bridged (inorganic) mixed-valence systems can be related to the constituent metal–ligand (and ligand–metal) coupling element (**H**) and the (reduced) energy gap (ΔE) between the metal and ligand redox orbitals. As applied to the wholly organic mixed-valence systems of interest here, the ligand-to-metal (LM) and metal-to-ligand (ML) are renotated as bridge-to-redox center (bD) and redox center-to-bridge (Db), respectively. According to the CNS model, the **D** to $\mathbf{D}^{+\bullet}$ (electronic) coupling element is then given by:[5,26]

$$\mathbf{H}_{CNS} = H_{Db}H_{D'b}/2\Delta E_{Db} + H_{bD}H_{bD'}/\Delta E_{bD} \qquad (2)$$

and a reduced energy gap, ΔE_{bD}, by:[5,26]

$$\Delta E_{bD} = [{}^1/_2\{1/E_{bDCT} + 1/(E_{bDCT} - E_{DDCT})\}]^{-1} \qquad (3)$$

where E_{bDCT} and E_{DDCT} are the energies of the bridge-to-redox center and intervalence transitions, respectively. In such a way, the intramolecular electron-transfer pathway is ascribed to the redox center-to-bridge charge transfer (DbCT), while the hole transfer is associated with bridge-to-redox center (bDCT).[27] Although the CNS model has been validated heretofore only for transition-metal systems, let us now see how it can be applied to the **D**-br-$\mathbf{D}^{+\bullet}$ system in Chart 1. In our mixed-valence system, we need consider only the bridge-to-redox center (bD) charge-transfer (super-exchange) mechanism owing to the intense ph $\rightarrow \mathbf{D}^{+\bullet}$ transition in the Vis/NIR spectral region, as described in Tables 3 and 4.[28] As such, only the second term in eq 2 is important, and the expression for the electronic coupling element reduces to

$$\mathbf{H}_{CNS} = H_{bD}{}^2/\Delta E_{bD} \qquad (4)$$

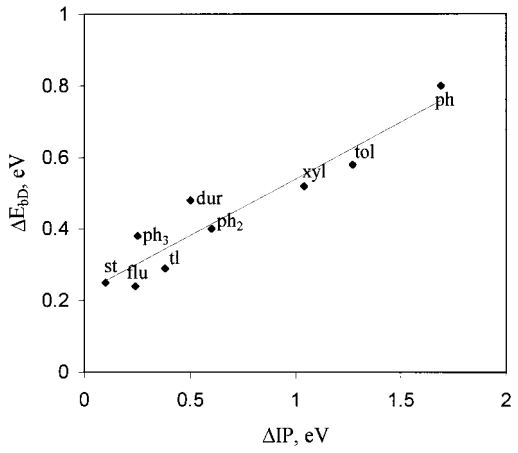

Figure 7. Correlation of the theoretical (**D**/br) energy gap (eq 3) in **D**-br-$\mathbf{D}^{+\bullet}$ with the experimental gap where ΔIP is the difference between the ionization potential of the bridge (taken as H-br-H) and that of the redox center (**D**-H).

TABLE 6: Creutz, Newton, and Sutin (CNS) Superexchange Model for the Calculation of Electronic Coupling Elements

MVS	r,[a] Å	IP,[b] eV	ν_{bDCT},[c] 10^3 cm^{-1}	$\mathbf{H}_{Db}$,[d] cm^{-1}	ΔE_r,[e] 10^3 cm^{-1}	$\mathbf{H}_{CNS}$,[f] cm^{-1}
PH	4.3	9.25	11.0	1413	6.5	307
TOL	4.3	8.83	10.5	1581	4.2	595
XYL	4.3	8.60	10.6	1148	4.2	310
DUR	4.3	8.06	10.6	546	3.9	77
PH_2	6.5	8.06	8.8	1530	3.3	701
PH_3	8.6	7.80	7.9	991	2.0	481
PH_4	10.8	8.08	7.8	846	1.9	
FL	6.5	7.80	7.6	1223	3.1	485
ER	7.1	–	9.4	930	2.9	298
TL	7.7	7.94	8.4	1116	2.4	528
BB	7.7	8.90	10. 0	1043	4.6	
ST	7.7	7.76	6.5	1450	2.0	1060

[a] Taken as half the value of r in Table 5. [b] Ionization potential of H-br-H taken from ref 21. [c] From Tables 3 and 4. [d] From eq 1 with r from column 2, ν_{bDCT} in column 4, and ϵ from Tables 3 and 4. [e] From eq 3. [f] From eq 4.

The energy gap for eq 4 is obtained from the Vis/NIR spectral data (in Tables 4 and 3), with (a) the energy of the bridge-to-redox center charge-transfer transition E_{bDCT} taken as the lowest-energy band of the dication **D**-br-$\mathbf{D}^{2+}$ and (b) the energy for the $\mathbf{D}/\mathbf{D}^{+\bullet}$ interaction E_{DDCT} taken as the intervalence band of the cation radical **D**-br-$\mathbf{D}^{+\bullet}$.[28] Figure 7 shows that the evaluated energy gap correlates with the electron-donor property of the bridge, as measured by the ionization potential of the dihydro derivative of the parent (H-br-H).

The values of the electronic coupling element $\mathbf{H}_{CNS}$ and the energy gap ΔE_{bD} (calculated from eqs 4 and 3 on the basis of the spectral data of the dication and using half of the distance between **D** centers for the separation parameter[5,26]) for the groups A–C systems are listed in the Table 6. The results show, that the electronic coupling elements obtained via the Mulliken–Hush and the Creutz, Newton, and Sutin treatments in Tables 5 and 6 respectively, mutually agree satisfactorily (generally within the factor of 2).[29] In both cases, the conformational effect of adding methyl substituents on the phenylene bridge, as well as the separation effect of multiple phenylene units, show the same trends in the diminishing magnitudes of **H**. Furthermore, the calculated energy gap ΔE_{bD} is well correlated with the difference in cylic voltammetric redox potentials of aromatic bridge prototypes (H-br-H) and the redox centers (**D**-H) in Figure 7.[30] Such indications in particular support the applicability of the CNS superexchange model; and since it derives from the phenylene bridge HOMO, we conclude that the hole-transfer mechanism pertains to the intramolecular electron-transfer process in the (poly)phenylene **D**-br-$\mathbf{D}^{+\bullet}$ mixed-valence systems.

TABLE 7: Electron–Exchange Thermodynamics from the Comproportionation Equilibrium: Comparison with the Theoretical Values (ΔE_r) from the MH and CNS Treatments

MVS	ΔE_{ox},[a] V	ΔE_r (MH),[b] V	ΔE_r (CNS),[c] V
PH	0.11	0.023	0.004
TOL	0.09	0.005	0.011
XYL	0.02	0.003	0.003
DUR	0	0.001	0.0002
PH_2	0	0.007	0.01
PH_3	0	0.002	0.009
PH_4	0	0	0
FL	0.06	0.02	0.01
ER	0	0.002	0.003
TL	0	0.004	0.01
ST	0	0.02	0.09
BB	0	0	0

[a] From Table 1. [b] Calculated from eq 6 and $\mathbf{H}_{MH}$ in Table 5. [c] Calculated from eq 6 and $\mathbf{H}_{CNS}$ in Table 6.

As a further (quantitative) evaluation of the MH and CNS theories for intramolecular electron transfer, let us determine how the calculated variation of the electronic coupling element **H** and the reorganization energy λ, as obtained from the electronic spectra, compare with the experimental (thermodynamics and kinetics) measurements.

III. Quantitative Evaluation of Electron-Transfer Thermodynamics and Kinetics. *A. Thermodynamics of the Comproportionation Equilibrium.* The electronic interaction between **D** and $\mathbf{D}^{+\bullet}$ redox centers in bridged mixed-valence systems is an important factor in the establishment of the comproportionation equilibrium,[1,26,31] i.e.,

$$\mathbf{D}\text{-}\mathbf{D}^{2+} + \mathbf{D}\text{-}\mathbf{D} \rightleftarrows \mathbf{D}\text{-}\mathbf{D}^{+\bullet} \qquad (5)$$

The free-energy change in such a reversible process, $\Delta G_{com} = -RT \ln K_{com}$, is made up of two principal components: ΔG_r the resonance stabilization arising from an electronic interaction (delocalization) and ΔG_{nr} a composite (nonresonance) contribution including solvation, entropy (statistical) factors, electrostatics, etc.[31] Since the latter is usually minor (and rather invariant),[1] we consider the free-energy change of comproportionation in eq 5 to be dominated by ΔG_r, which for Robin–Day class II systems can be calculated as[26,31]

$$\Delta G_r = -2\mathbf{H}^2/\lambda \qquad (6)$$

Experimentally, ΔG_{com} for the comproportionation equilibrium is taken as the difference ΔE_{ox} in the reversible oxidation potentials E_1 and E_2 for the successive 1e oxidation of the **D**-br-**D** donor to its cation radical and then to the dication, respectively; so that $\Delta G_r = -\mathcal{F}\Delta E_{ox}$, where $\mathcal{F}$ is the Faraday constant. Table 7 compares the experimentally obtained values of ΔE_{ox} (second column) with the theoretically calculated[1] values of ΔE_r via the MH and CNS treatments (third and fourth columns) for the series of groups A–C mixed-valence systems in Chart 1.

For those mixed-valence systems in which the energy gap is too narrow to be measured reliably (i.e., $\Delta E_{ox} \sim 0$) the theoretically values (by both MH and CNS methods) are also less than 0.01 V, i.e., too small to be seen and in agreement with the experimental data. Otherwise, the theoretical values of ΔE_r are significantly less than the experimental values, even in those systems for which ΔE_{ox} is experimentally meaningful. Part of the discrepancy may be attributed to an underestimation of **H** (from the spectral data)[32] and/or necessity of including

TABLE 8: Comparison of Electron-Transfer Rate Constants from ESR Line Broadening and the Theoretical Predictions of the Mulliken−Hush (MH) and the Creutz, Newton, and Sutin (CNS) Formalisms

MVS	$\Delta G^{\neq}_{CNS}$,[b] kcal/M	$\Delta G^{\neq}_{MH}$,[a] kcal/M	k_{ET} (−100 °C), s^{-1}			k_{ET} (20 °C),[c] s^{-1}		
			CNS	MH	ESR	CNS	MH	ESR
PH	3.7	2.6	2×10^7	5×10^8	10^{10}	2×10^9	1×10^{10}	$>10^{10}$
TOL	4.1	4.6	8×10^6	2×10^6	5×10^6	1×10^9	4×10^8	$10^{8,9}$
XYL	4.8	4.8	9×10^5	9×10^5	$<3 \times 10^6$	3×10^8	3×10^8	10^8
DUR	5.7	5.4	7×10^4	2×10^5	$<3 \times 10^6$	6×10^7	9×10^7	10^8
PH_2	3.1	3.7	1×10^8	2×10^7	2×10^7	6×10^9	2×10^9	3×10^9
PH_3	3.5	4.2	4×10^7	6×10^6	5×10^6	2×10^9	8×10^8	1×10^8
PH_4[d]	4.8	4.8	1×10^6	1×10^6	$<3 \times 10^6$	3×10^8	3×10^8	3×10^7
FL	4.0	2.4	9×10^6	9×10^8	5×10^7	1×10^9	2×10^{10}	$10^{8,9}$
ER	4.6	4.6	2×10^6	2×10^6	$<3 \times 10^6$	4×10^8	4×10^8	$10^{8,9}$
TL	3.6	4.1	3×10^7	6×10^6	5×10^6	2×10^9	9×10^8	10^8
ST	1.4	2.2	2×10^{10}	2×10^9	$10^{8,9}$	1×10^{11}	2×10^{10}	$10^{8,9}$
BB[e]	5.0	5.0	5×10^5	5×10^5	$<3 \times 10^6$	2×10^8	2×10^8	5×10^7

[a] From eq 7, $\lambda = \nu_{IV}$ and $\mathbf{H}_{MH}$ from Table 5. [b] From eq 7, $\lambda = \nu_{IV}$ and $\mathbf{H}_{CNS}$ from Table 6. [c] For limitation on the precision of k_{ET} (especially at high temperature), see Discussion. [d] λ taken to be the same as in $\mathbf{D}(ph)_3\mathbf{D}^{+\bullet}$ and $\mathbf{H}$ is neglected. [e] λ taken to be the same as in $\mathbf{D}(tl)\mathbf{D}^{+\bullet}$ and $\mathbf{H}$ is neglected.

nonresonance contributions which can take on increasing (relative) importance in the case of weakly interacting $\mathbf{D}/\mathbf{D}^{+\bullet}$ centers. Be that as it may, the limited correlation of theoretically based $\mathbf{H}_{MH}$ and $\mathbf{H}_{CNS}$ with the experimental results do not allows us to come to more definite conclusions, based on the *thermodynamic* considerations in eq 6.

B. Kinetics from the ESR Line Broadening. The activation free energy for intramolecular electron transfer in Robin−Day class II systems is given by[1,33]

$$\Delta G^{\neq} = (\lambda - 2\mathbf{H})^2/4\lambda \qquad (7)$$

and the theoretical values of $\Delta G^{\neq}$ based on the reorganization energy λ and the values of $\mathbf{H}_{MH}$ and $\mathbf{H}_{CNS}$ calculated by the Mulliken−Hush and the Creutz, Newton, and Sutin formalism, respectively, are presented in the Table 8. The general trends are for both $\Delta G^{\neq}_{MH}$ and $\Delta G^{\neq}_{CNS}$ (increasing with the number of methyl substituents and with the number of phenylene units in groups A and B cation radicals, respectively), to follow the qualitative expectations developed from the conformation and distance effects presented above.

For a more quantitative comparison, we consider the first-order rate constant k_{ET} for the electron transfer obtained from the line broadening of the ESR spectra recorded at high (20 °C) and at low (−100 °C) temperatures in Figures 1−3. On the basis of the calculated values of $\Delta G^{\neq}$, the rate constant expression:[33] $k = k_{el}\nu_n \exp(-\Delta G^{\neq}/RT)$ was simplified so that a common preexponential factor of $k_{el}\nu_n = 10^{12}$ s^{-1} was taken for all groups A−C mixed-valence systems.[1] The results in Table 8 show a general agreement between the experimental and the calculated rate constants (within an order of magnitude) at both high and low temperatures.[34] The largest discrepancies lie with the mixed-valence systems containing the phenylene (ph) and fluorenyl (flu) bridges which could result from the values of $\Delta G^{\neq}_{CNS}$ which are too high as a result of underestimation of $\mathbf{H}_{CNS}$. The CV and ESR data also imply higher values of the electronic coupling elements in these mixed-valence cations (vide supra).[35] Although the ESR measurements generally confirm the calculated kinetics (based on the electronic spectra), clearly more detailed ESR studies yielding precise measurements of k_{ET} are required before a definitive choice can be made between MH and CNS-based electronic coupling elements.

IV. Bridge effects of Phenylene *Conformation*, Separation *Distance*, and Electronic *Connectivity* on Intramolecular Electron Transfer. There is general agreement of the experimental (electron-transfer) kinetics with either the Mulliken−Hush or the Creutz, Newton, and Sutin (CNS) treatment of the electronic coupling elements between $\mathbf{D}/\mathbf{D}^{+\bullet}$ redox centers in the mixed-valence cation radicals (Chart 1). However, the CNS formalism does provide the mechanistic basis for the intramolecular electron transfer directly via the bridge/donor interface; and we thus employ eqs 2 and 3 to evaluate the conformation, distance and connectivity effects of the (poly)phenylene bridges on intramolecular electron transfer as follows.

X-ray analysis of the $\mathbf{D}(ph)\mathbf{D}^{+\bullet}$ donor and its cation radical indicates that significant planarization[10] occurs between the benzenoid redox center (**D**) and the phenylene (ph) bridge upon 1e removal − the dihedral angle diminishing from $\varphi = 45°$ to ∼30°. This conformational effect is accompanied by tightening of the **D**-ph bond from 1.493 to as much as 1.474 Å.[1] Such a coplanarization/shortening of the bond between the redox center and the bridge is an indication of increasing $\pi-\pi$ conjugation between the two moieties.[10] Since the effectiveness of π-conjugation is highly dependent on the dihedral angle (φ), it can be strongly suppressed by the deliberate control of the molecular conformation, such as the introduction of as many as four methyl groups in the phenylene bridge.[36] This conformational effect is undoubtedly responsible for (a) the dramatic decrease in the electronic coupling element ($\mathbf{H}_{MH}$ and $\mathbf{H}_{CNS}$) in $\mathbf{D}(dur)\mathbf{D}^{+\bullet}$ from that in the parent (see Tables 5 and 6) and (b) the relatively slow rates of intramolecular electron transfer (Table 8). The latter pertains despite the fact that methyl substitution results in an increased HOMO energy of the tetramethylated phenylene bridge[21,37] that would otherwise lead to a more (not less) effective **D**/br electronic interaction. In other words, the bridge *conformation* is significantly more important than the orbital energy of the bridge in facilitating the intramolecular electron transfer in phenylene based mixed-valence systems.

Increased separation of $\mathbf{D}/\mathbf{D}^{+\bullet}$ redox centers that (expectedly) impact negatively on intramolecular electron-transfer rates (Table 8) are theoretically seen as diminishing values of the electron coupling elements (Table 6). Distance by itself however is not the ameliorating factor since $\mathbf{H}_{CNS}$ for the biphenylene $(ph)_2$-bridged system is substantially greater than that of the tetramethylphenylene (or the aliphatic trimethylene[1]) bridged analogue(s), in which the distance parameter r is as much as 3 Å closer. The enhanced possibility of π-conjugation deriving from less (**D**/br) steric hindrance[38] in $\mathbf{D}(ph)_2\mathbf{D}^{+\bullet}$ relative to $\mathbf{D}(dur)\mathbf{D}^{+\bullet}$ is clearly more important than decreasing the distance between redox centers for intramolecular electron transfer. Moreover, the conformational effect is improved further by the

addition of the bifunctional $-(CH_3)_2C-$ tie to complete the coplanarization of the biphenylene bridge,[39] as in the **D**(flu)-**D**$^{+\bullet}$ mixed-valence system. X-ray structural analysis of **D**(flu)-**D**$^{+\bullet}$ shows that the smaller dihedral angles[39] between **D**/flu planes lead to an increase in the magnitude of ΔE_{ox} (Table 7) and a more intense NIR absorption compared to those in **D**(ph)$_2$**D**$^{+\bullet}$. As a result, the larger calculated value of $\mathbf{H}_{MH}$ is consistent with the enhanced conjugation attendant upon such a forced planarization.[40,41]

The separation distance is even less important as seen by the insertion of an ethylenic ($-CH=CH-$) linkage between the phenylene units in the biphenylene bridge. Thus the electronic coupling element $\mathbf{H}_{CNS}$ for the stilbenoid bridged cation radical **D**(st)**D**$^{+\bullet}$ is the highest of all the groups A−C systems, and even higher than that of the fluorenyl analogue (Table 6). Again π-conjugation is an important factor since the electronic coupling element in the acetylenic ($-C\equiv C-$) bridged cation radical **D**(tl)-**D**$^{+\bullet}$ is only slightly less—the saturated alkylidene ($-CH_2CH_2-$) by far the least effective of all. Finally, the loss of π-conjugation through the insulating (saturated alkylidene) insert results in the disappearance of the critical br/**D**$^{+\bullet}$ charge-transfer (absorption) band in toto.

Summary and Conclusion

The Creutz, Newton, and Sutin (CNS) superexchange model is shown for the first time to correctly predict intramolecular electron-transfer rates (k_{ET}) between wholly organic redox centers in mixed-valence systems **D**-br-**D**$^{+\bullet}$ with various types of phenylene bridges (br). Analysis of the intervalence (NIR) absorption bands yields more or less reliable values of the electronic coupling element ($\mathbf{H}_{CNS}$), in which the hole-transfer pathway pertains to the superexchange mechanism between the bridge (phenylene) HOMO and the paramagnetic (**D**$^{+\bullet}$) redox center. Structural control of the molecular conformation between the planar redox center and the (phenylene) bridge is critical for modulating the electronic coupling element. The latter is achieved by (a) adjustment of the number of methyl substituents and (b) coplanarization of the biphenylene bridge with the bifunctional $-(CH_3)_2C-$ tie, which in both cases result in effective through π-conjugation between **D**/**D**$^{+\bullet}$ centers. Such a stereochemical effect can dominate other factors such as the (orbital) energetics and the (separation) distance between redox centers.

Experimental Section

I. Materials. 4,4″-dimethyl-2,5,2″,5″-tetramethoxy-1,1′:4′,1″-terphenyl (**D**(ph)**D**), 4,4‴-dimethyl-2,5, 2‴,5‴-tetramethoxy-1,1′:4′,1″:4″,1‴-quaterphenyl (**D**(ph)$_2$**D**), 4,4⁗-dimethyl-2,5,2⁗,5⁗-tetramethoxy-1,1′:4′,1″:4″,1‴:4‴,1⁗-quinquiphenyl (**D**(ph)$_3$**D**) 4,4⁗-dimethyl-2,5,2⁗,5⁗-tetramethoxy-1,1′: 4′,1″:4″,1‴:4‴,1⁗:4⁗,1⁗-sexaphenyl (**D**(ph)$_4$**D**), 4,2′,4″-trimethyl-2,5,2″,5″-tetramethoxy-1,1′:4′, 1″:4″,1‴-terphenyl (**D**(tol)**D**), 4,2′,5′,4″-tetramethyl-2,5,2″,5″-tetramethoxy-1,1′:4′,1″:4″,1‴-terphenyl (**D**(xyl)**D**), 4,2′3′,5′,6′,4″-hexamethyl-2,5,2″,5″-tetramethoxy-1,1′:4′,1″-terphenyl (**D**(dur)**D**), 2,7-bis(4,4″-dimethyl-2,5,2″,5″-tetramethoxy-benzene)-9,9′-dimethyl-fluorene, (**D**(flu)**D**), 4,4′-bis(2,5-dimethoxy-4-methylphenyl)-tolan (**D**(tl)**D**), 4,4′-bis(2,5-dimethoxy-4-methylphenyl)-bibenzyl (**D**(bb)**D**), *trans*-4,4′-bis(2,5-dimethoxy-4-methylphenyl)-stilbene (**D**(st)**D**), 2,5-dimethoxy-4-methyl-1,1′-biphenyl (**D**phH), 2,5-dimethoxy-4-methyl-1,1′:4′,1″-terphenyl (**D**(ph)$_2$H), 2,5-dimethoxy-4-methyl-1,1′:4′,1″:4″,1‴-quaterphenyl (**D**(ph)$_3$H were prepared as published,[10] as well as the precursor of 2,3,8,9-tetrahydro-1,1,4,4,7,7,10,10-octamethyltetracene radical cation (**OMN**$^{+\bullet}$).[41] All of the compounds were characterized by melting points, IR, ^{1}H NMR, ^{13}C NMR, mass spectroscopies, and elemental analysis. Dichloromethane and toluene were purified according to published procedures.[42]

II. Instrumentation. The ^{1}H NMR spectra were recorded in $CDCl_3$ on a General Electric QE-300 NMR spectrometer. Infrared spectra were recorded on a Nicolet 10 DX FT spectrometer. Gas chromatography was performed on a Hewlett-Packard 5890A gas chromatograph equipped with a HP 3392 integrator. GC-MS analyses were carried out on a Hewlett-Packard 5890 gas chromatograph interfaced to a HP 5970 mass spectrometer. X-ray crystallographic analysis was carried out with aid of a Siemens SMART diffractometer equipped with a CCD detector using Mo Kα radiation ($\lambda = 0.71073$ Å), at −150 °C. Procedures for the X-ray crystallographic analysis (and crystal data) (see Supporting Information) of the neutral donors and cation radicals salts were described previously.[1,10]

Cyclic voltammetry was performed on a BAS 100A electrochemical analyzer. The measurements were carried out at a uniform sweep rate of 2 V s^{-1} in a solution of 0.1 M supporting electrolyte (tetra-*n*-butylammonium hexafluorophosphate) and 5×10^{-4} M compound in dry dichloromethane under an argon atmosphere. The working electrode consisted of an adjustable platinum disk embedded in a glass seal with ~1 mm^2 surface area. The potentials were referenced to SCE (separated from the cathode by a sintered glass frit), which was calibrated with added ferrocene (5×10^{-4} M). Controlled-potential coulometry was conducted with an EG&G Princeton Applied Research (PAR) 173 potentiostat and digital coulometer as described.[10]

III. General Procedure for the UV−vis−NIR Spectroscopic Characterization of Cation Radicals. All electronic spectra were recorded with a Cary 500 UV−vis−NIR spectrometer. Spectra of the cation radicals **D**(ph)$_n$H$^{+\bullet}$ ($n = 1-4$) were obtained by adding 1 equiv of the 1e oxidant **OMN**$^{+\bullet}$SbCl$_6^-$ ($E^o_{red} = 1.34$ V vs SCE, generated in *situ* by the addition of nitrosonium salt $NOSbCl_6$ in anhydrous dichloromethane) to the solution of neutral donor. Spectra of the cation radical **D**-br-**D**$^{+\bullet}$ and the dication **D**-br-**D**$^{2+}$ were obtained by spectral titration as follows. A 1-cm quartz cuvette equipped with a Schlenk adaptor was charged under an argon with 3 mL of a freshly prepared solution of **OMN**$^{+\bullet}$ SbCl$_6^-$. The concentration of the oxidant (usually near 0.1 mM) was based on the absorbance at 673 nm.[43] A solution of 10 mM donor (**D**-br-**D**) in dichloromethane was added to the oxidant solution in 3 μL increments. At the beginning of the titration, the intensity of the 673-nm band decreased and a low-energy band (centered, depending on the br, at λ_{max} from 900 to 1500 nm, see λ_2 in Tables 3 and 4) was formed with increasing intensity, and the isosbestic point was observed. The absorption decrease at 673 nm and the low-energy absorption band increase (with the isosbestic point between) were proportional to the amount of the added donor until 15 μL of donor solution was added. At this juncture, the added donor corresponds to $^1/_2$ equiv of the oxidant, indicating the 1 equiv of **OMN**$^{+\bullet}$ reacted with $^1/_2$ equiv of neutral donor to form the dication

$$^1/_2\mathbf{D}\text{-br-}\mathbf{D} + \mathbf{OMN}^{+\bullet} \rightarrow {}^1/_2\mathbf{D}\text{-br-}\mathbf{D}^{++} + \mathbf{OMN} \qquad (8)$$

This spectrum was taken as the spectrum of the dication, **D**-br-**D**$^{++}$. As the titration was continued, the intensity of the band centered at 673 nm remained invariant, and the intensity increase of the low-energy band diminished. The absorption maximum was red-shifted. Another isosbestic point was observed, and the absorption in the low energy region (1500 nm−2200 nm) increased indicating the comproportionation reaction between

the dication and the neutral donor to reversibly generate the cation radical

$$\mathbf{D}\text{-br-}\mathbf{D}^{++} + \mathbf{D}\text{-br-}\mathbf{D} \rightleftarrows \mathbf{D}\text{-br-}\mathbf{D}^{+\bullet} \qquad (9)$$

After 4 equiv of the donor was added, the spectrum was invariant and taken to be that of the cation radical **D**-br-**D**$^{+\bullet}$. At this point, the comproportionation equilibrium was greatly shifted to the right, and the amount of the dication was spectroscopically negligible.

For the distances between the redox centers *r* in the MVS for the Mulliken−Hush electronic coupling elements calculation (eq 1), the separation between the centers of the dimethoxybenzene rings was used. The values of *r* were determined with the aid of computer program for molecular mechanics calculations Alchemy. Satisfactory correspondence (±1−2%) between the values determined in such a way values with the data available from X-ray measurements [for **D**(ph)**D**$^{+\bullet}$, **D**(ph)$_2$**D**$^{+\bullet}$, and **D**(flu)**D**$^{+\bullet}$] confirms the reliability of the calculated distances.

IV. ESR Spectra of the Mixed-Valence Cation Radicals. The cation radicals for the ESR study were generated from freshly prepared solution of **OMN**$^{+\bullet}$$SbCl_6$ in anhydrous dichloromethane as described above. The spectra were obtained from a Varian E-line Century Series ESR spectrometer from +20 to −100 °C. Static ESR spectra simulations were carried out with PEST WinSim program, version 0.96 (Public EPR Software Tools, National Institute of Environmental Health Sciences), by variation of the hyperfine splitting parameters and line widths to obtain the best correspondence of the simulated and the calculated spectra, starting from the parameters for the parent $DCH_3^{+\bullet}$.[44] Dynamic ESR spectra simulations were carried out with the aid of the ESR-EXN program.[45] In these cases, the parameters obtained in static ESR simulation for the mononuclear model cation radical were used as starting point, and the rate constants were varied to obtain the best correspondence between the calculated and experimental spectra.

The electron-transfer rate constant (k_{ET}) in Table 2 obtained from the ESR line-broadening experiments were most reliable in the rather narrow range: $3 \times 10^6 < k_{ET} < 10^8$ s^{-1}. At slower rates, the line broadening was insufficient to be observed; and at faster rates the line broadening was too severe. For example in the low-temperature experiments, a rate constant of $k_{ET} < 3 \times 10^6$ s^{-1} yielded a calculated spectrum that closely approximated the static ESR spectrum. At the high-temperature extreme, a rate constant of $k_{ET} \sim 10^{8.9}$ s^{-1} was indicated by a single broadened line (which showed additional splittings at both faster and slower rates). At $k_{ET} \approx 10^8$ s^{-1} the single broadened line showed some slight (but unresolved) splittings. For the ESR behavior of the fluorenyl-bridged cation **D**(flu)**D**$^{+\bullet}$, an additional small hyperfine splittings of $a_{6H} = 1.1$ G for a pair of methyl groups provided an optimum simulation. For the stilbenoid analogue**,** the additional splittings were also required for the simulation of the unresolved envelope.

Acknowledgment. We thank Professor S. F. Nelsen for kindly providing the ESR-EXN simulation program, R. Rathore for carrying out some initial studies,[10] and the R.A. Welch Foundation and National Science Foundation for financial support.

Supporting Information Available: X-ray crystallographic data for the bridge mixed-valence systems **D**(flu)**D**$^{+\bullet}$ and **D**(dur)**D** (Tables S1−S10). This material is available free of charge via the Internet at http://pubs.acs.org.

References and Notes

(1) Lindeman, S. V.; Rosokha, S. V.; Sun D.-L.; Kochi, J. K. *J. Am. Chem. Soc.* **2002**, *124*, 843.

(2) (a) Mulliken, R. S.; Person, W. B. *Molecular Complexes*; Wiley: New York. 1969. (b) Hush, N. S. *Prog. Inorg. Chem.* **1967**, *8*, 391. (c) Hush, N. S. *Electrochim. Acta*. **1968**, *13*, 1005.

(3) Creutz, C. *Prog. Inorg. Chem.* **1983**, *30*, 1.

(4) For the few (earlier) studies of organic mixed-valence system that addressed the role of the bridge conformation, length and connectivity, see: (a) Nelsen, S. F.; Ismagilov, R. F.; Powell, D. R. **1997**, *119*, 10213. (b) Nelsen, S. F.; Ismagilov, R. F.; Powell, D. R. *J. Am. Chem. Soc.* **1998**, *120*, 1924. (c) Nelsen, S. F.; Ismagilov, R. F.; Gentile, K. E.; Powell, D. R. *J. Am. Chem. Soc.* **1999**, *121*, 7108. (d) Lambert, C.; Nöll, G. *J. Am. Chem. Soc.* **1999**, *121*, 8434.

(5) (a) Creutz, C.; Newton, M. D.; Sutin, N. *J. Photochem. Photobiol. A: Chem.* **1994**, *82*, 47. (b) For the classification of a mixed-valence systems as class II, see: Robin, M. B.; Day, P. *Adv. Inorg. Chem. Radiochem.* **1967**, *10*, 247.

(6) Structural changes in groups A−C donors and their cation radicals were generally too small for effective quantification by X-ray crystallography.

(7) The resonance interaction ΔE_{ox} is measured as the potential difference between the first and second CV waves in Table 1, columns 3 and 4. For a discussion, see ref 1.

(8) Estimated owing to the partially resolved (first and second) CV waves.

(9) For the evaluation of k_{ET} from the temperature-dependent line-broadening, see ref 1.

(10) Sun, D.-L.; Lindeman, S. V.; Rathore, R.; Kochi, J. K. *J. Chem. Soc., Perkin Trans. 2* **2001**, 1585.

(11) The local bands of the **D**$^{+\bullet}$ redox center lie in the 400−500 nm region with a weak band at 700 nm.

(12) (a) For analogous NIR transitions in the *inter*molecular (π-dimeric) complexes of aromatic cation radicals and donors, see: Kochi, J. K.; Rathore, R.; Zhu, C.-J.; Lindeman, S. V. *J. Org. Chem.* **2000**, *112*, 3671 and Le Maqueres, P.; Lindeman, S. V.; Kochi, J. K. *J. Chem. Soc., Perkin Trans. 2* **2000**, 1180. (b) Analogous (pairwise) transitions have been observed in other organic mixed-valence systems. See Nelsen et al. in ref 4b.

(13) The 2e oxidations of the **D**-br-**D** donors afford persistent dications that contain a pair of terminal cation radical centers, and are thus otherwise described as dication diradicals.[10]

(14) For the other analogues with $n = 3$ and 4, the serious (band) overlaps precluded the resolution of meaningful intervalence absorptions.

(15) Compare also Nelsen et al. in ref 4b.

(16) For example, the first and second ionization potentials of toluene are 8.83 and 9.36 eV, for *p*-xylene they are 8.67 and 9.15 eV, for biphenyl they are 8.34 and 9.04 eV, and for stilbene (vide infra) they are 7.87 and 9.08 eV.[17]

(17) See: Traven, V. F. *Frontier Orbitals and Properties of Organic Molecules*; Ellis Horwood: N.Y. 1992.

(18) Howell, J. O.; Goncalves, J. M.; Amatore, C.; Klasinc, L.; Wightman, R. M.; Kochi, J. K. *J. Am. Chem. Soc.* **1984**, *106*, 3968.

(19) Note that normalized absorbances of **D**(ph)$_n$**D**$^{+\bullet}$, **D**(ph)$_n$**D**$^{2+}$, and **D**(ph)$_n$H$^{+\bullet}$ ($n = 3$ and 4) are roughly the same.

(20) The ionization potential of the bridge in FL is expected to be lower than that of fluorene (7.80 eV)[21] by the extent of dialkyl substituents.

(21) See: http://www.webbook.nist.gow.

(22) Bandwidths (fwhm) were obtained by the deconvolution procedure and are presented in Table 5, column 4.

(23) X-ray structural analysis of the FL cation radical shows unequal geometry of the terminal **D** groups that lead to quinonoidal distortions corresponding to +0.20 and +0.35 fractional positive charges, the remainder (+0.45) being associated with the fluorenyl bridge.[10]

(24) A relatively large electronic interaction between the redox center **D** and the fluorenyl bridge (flu) must also be considered.

(25) Eberson, L.; Hartshorn, M. P.; Radner, F.; Persson, O. *J Chem. Soc. Chem. Commun.* **1996**, 215. The energy difference between the cation radical states with the positive charge located on **D** and that on the (stilbenoid) bridge in ST$^{+\bullet}$ is even less than that in FL$^{+\bullet}$ owing to the oxidation potential of stilbene that is less than that of fluorene. Although we have no X-ray structure data on the ST$^{+\bullet}$, its ESR spectra were broadened at all temperatures (20 to −100 °C) and the computer simulation required the inclusion of additional hyperfine splittings (as an indication of the localized charge on the bridge).

(26) Evans, C. E. B.; Naclicki, M. L.; Rezvani, A. R.; White, C. A.; Kondratiev, V. V.; Crutchley, R. J. *J. Am. Chem. Soc.* **1998**, *120*, 13096.

(27) (a) Generally the energetics (being as they are) will cause one superexchange mechanism to be dominant in a given mixed-valence system.[26] (b) Furthermore, this situation applies especially to organic mixed-valence systems owing to the relative spacings of p (and s) orbitals.

(28) (a) The most unambiguous assignment of the bridge-to-redox center charge transfer derives from the VIS−NIR bands in the dication (in which each center is formally $\mathbf{D}^{+\bullet}$[10]). Here we employ only the lowest-energy band since the inclusion of the penultimate band did not materially affect the calculated value of **H** because its value of ΔE_{bD} is substantially larger. (b) The electronic coupling element for the bridge-to-redox center $\mathbf{H}_{bD}$ is obtained from the eq 1 with ν_{CT} of the bDCT band evaluated from Table 4 (column 5).

(29) The largest deviations were observed with the bridged br = ph, flu and st owing to the relatively large values of **H** which preclude their consideration as weakly interacting systems. The agreement of $\mathbf{H}_{MH}$ and $\mathbf{H}_{CNS}$ to within a factor of 2 is not uncommon (see refs 5 and 26).

(30) Note the close correspondence between the relative values of the gas-phase ionization potential (IP) and the oxidation potential ($E°_{ox}$) in solution for similarly constituted donors.[18]

(31) See: Astruc, D. *Electron Transfer and Radical Processes in Transition-Metal Chemistry*; VCH: New York, 1995.

(32) As presented and discussed for $\mathbf{D}(ph)\mathbf{D}^{+\bullet}$ in the previous paper.[1]

(33) Based on Marcus theory, as discussed by Sutin: (a) Sutin, N. *Prog. Inorg. Chem*. **1983**, *30*, 441. (b) Brunschwig, B. S.; Sutin, N. *Coord. Chem. Rev.* **1999**, *187*, 233.

(34) We note the experimental difficulties in obtaining precise rate constants from ESR data with some mixed-valence cation radicals, particularly at the (relatively) slow and very fast limits. Thus, the limited line broadening for $k_{ET} < 10^6$ s^{-1} and severe line broadening at $k_{ET} > 10^8$ s^{-1} were difficult to simulate with precision.

(35) In addition, the significant charge density on the flu and st bridges suggests that the use of the two-state model may require modification.

(36) Unfortunately, we were unable to grow single crystals of the tetramethylated cation radical ($DUR^{+\bullet}$) for X-ray crystallography. However the perpendicular conformation ($\varphi = 90°$) extant in the neutral donor $\mathbf{D}$(dur)-$\mathbf{D}$[10] suggests that the dur/**D** planes are also (nearly) orthogonal in the cation radical.

(37) See Howell. J. O. et al. in ref 18.

(38) In $\mathbf{D}(ph)_2\mathbf{D}$, the bridge/donor dihedral angles of $\varphi = 31$ (and 36)° compare with the intercyclic angle of $\varphi = 17°$, and a shortened bond of 1.47 Å compared with 1.49 Å in the neutral donor.[10]

(39) The dihedral angles between the redox center **D** and the flu bridge are reduced to $\varphi = 30°$, and the intercyclic angle is drastically reduced to $\varphi = 6°$ by the addition of the $-(CH_3)_2C-$ tie.[10]

(40) (a)Note the spectral similarities of the corresponding dications. However, the increased charge distribution in the flu bridge may render the two -state model inappropriate (vide supra), which could render the calculation of the ET rate constant (based on $\mathbf{H}_{CNS}$) to be unreliable. (b) Note that the experimental (at −100 °C) and calculated values (based on $\mathbf{H}_{MH}$) of the rate constants k_{ET} for $\mathbf{D}(flu)\mathbf{D}^{+\bullet}$ are higher than those for $\mathbf{D}(ph)_2\mathbf{D}^{+\bullet}$ (see Tables 2 and 8). Unfortunately, the experimental rate constants at higher temperature (20 °C) were not compared owing to low accuracy.

(41) Rathore, R.; Kumar, A. S.; Lindeman, S.; Kochi, J. K. *J. Org. Chem.* **1998**, *63*, 5847.

(42) Perrin, D. D.; Armagero, W. L.; Perrin, D. R. *Purification of Laboratory Chemicals*, 2nd ed; Pergamon: New York, 1980.

(43) Rosokha, S. V.; Kochi, J. K. *J. Am. Chem. Soc*. **2001**, *123*, 8985.

(44) Forbes, W. F.; Sullivan, P. D. *J. Phys. Chem*. **1968**, *48*, 1411.

(45) Heinzer, J. Quantum Chemistry Program Exchange 209, as modified by Petillo, P. A. and Ismagilov, R. F., Chemistry Dept., Indiana Univ., Bloomington, IN. We thank Prof. S. F. Nelsen for a copy of this program.